🔓**Open Access**

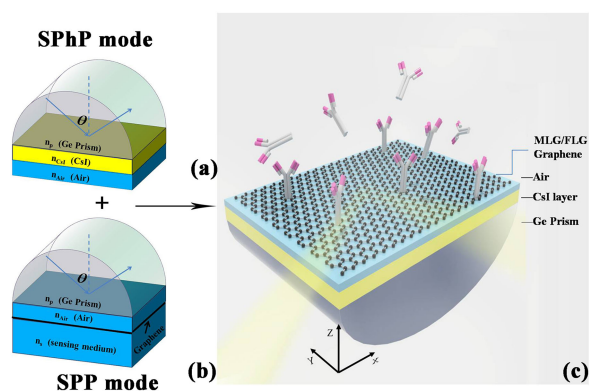# Ultrasensitive Terahertz Imaging Sensors Based on the Strong Coupling of Surface Phonon Polariton and Graphene Surface Plasmon Polariton

Jiaqi Zhu
Banxian Ruan
Qi You
Leiming Wu
Houzhi Cai
Xiaoyu Dai
Yuanjiang Xiang

Ultrasensitive Terahertz Imaging Sensors Based on the Strong Coupling of Surface Phonon Polariton and Graphene Surface Plasmon Polariton

Jiaqi Zhu [1,2] **Banxian Ruan,**[1,2] **Qi You,**[1,2] **Leiming Wu,**[1,2]
Houzhi Cai,[1] **Xiaoyu Dai,**[1,2] **and Yuanjiang Xiang** [1,2]

[1]Key Laboratory of Optoelectronic Devices and Systems of Ministry of Education and Guangdong Province, College of Optoelectronic Engineering, Shenzhen University, Shenzhen 518060, China
[2]International Collaborative Laboratory of 2D Materials for Optoelectronic Science & Technology of Ministry of Education, College of Optoelectronic Engineering, Shenzhen University, Shenzhen 518060, China

Abstract: Surface plasmon polaritons (SPPs) with noble metals lose the capacity to confine the optical field in the long wavelength region, while surface phonon polaritons (SPhPs) in polar dielectrics show greater ability to achieve high local field, sub-diffraction confinement, and low optical losses in the mid-IR to THz spectral ranges. We propose a hybrid structure based on SPhPs mode with CsI and SPPs mode with graphene in THz spectral ranges. The characteristics of the coupling of these two modes have been analyzed and strong coupling has been confirmed theoretically. The results are applied to an intensity-interrogated terahertz sensor; the highest imaging sensitivity as high as 954 RIU^{-1} and a large figure of merit of 74 740 RIU^{-1} have been demonstrated. The results could find potential applications in gas detection in the THz band.

Index Terms: Surface plasmon resonance, surface phonon polaritons (SPhPs), terahertz sensor, graphene.

1. Introduction

Terahertz (THz) wave is considered as the frequency of electromagnetic wave ranging from 0.1–10 THz (wavelength 30 μm–3 mm). Its long waveband is connected with a millimeter wave (sub-millimeter wave) and the short waveband is connected with infrared (far-infrared). Terahertz waves have a wide range of applications due to their unique "fingerprint" properties, transient nature, high penetration, broadband, coherence, and low energy characteristics, such as in communications, radar, and astronomy, medical imaging, biochemical identification, materials science, security inspections and other fields [1]–[4]. However, similar to other electromagnetic spectrums,

the diffraction limit problem of terahertz waves also restricts the miniaturization and integration of terahertz photonic devices. To emphasize an important point, the binding ability of surface plasmon wave is weak at the simple metal/medium structure in the Terahertz band, which is almost identical to free-propagating electromagnetic waves, they do not have the ability to overcome the diffraction limit. It is necessary for us to look for alternatives due to this point, such as metal superstructure materials, two-dimensional Dirac materials, and other types of surface polarization, for instance, surface phonon polariton.

It is known that phonon polariton is caused by the coupling between the phonon and electromagnetic field (photon). As one of the three main types polaritons: plasmon polariton, exciton-polariton and phonon polariton [5], whether or not an electromagnetic field is applied, the phonon-polariton is the intrinsic mode of polar materials. The fundamental natural lattice vibration frequency (ω_{TO}) of the actual crystal is generally located in the 10^{12}–10^{14} THz range (corresponding the mid-infrared and terahertz spectrum), but the response of natural materials in terahertz band is very limited, such as GaAs, InP, CaF_2 and so on [6]–[8]. On the one hand, surface phonon polariton behaves the function of overcoming the electromagnetic wave diffraction limit in mid-IR and terahertz waves. On the other hand, surface phonon polariton performs best in the aspect of low loss. The life of the surface polariton depends on the life of the polariton, and the lifetime of surface phonon polariton mode is one to two orders of magnitude longer than that of surface plasma polariton mode. From this point of view, the low loss of surface phonon polariton makes the application prospect more attractive.

Surface plasmon polariton (SPP) is a type of elementary excitation which is contributed to the electromagnetic wave resonates with the charge oscillation on the surface of the material. Over the past few years, the research of SPP chiefly centers on precious metals, for instance, gold (Au) and silver (Ag) can excite SPP in the visible and NIR (near-infrared) band due to the collective oscillation properties [9]–[11]. It is fewer for the research of SPP device in mid-infrared and terahertz spectrum, the vast majority of the researcher make a great endeavor in designing a high tunability and low losses and good performance SPP devices. In recent studies, researchers have proved the existence of SPP for graphene and its micro-nano structure turn into a rising star in the terahertz spectrum [12], [13]. As is known to all, metal can support SP mode only the real parts of permittivity is negative, according to the dielectric constant of graphene [14], graphene has negative permittivity when the imaginary component of conductivity is positive, which has many potential applications in Surface plasmon resonance (SPR) sensor. For example, Triranjita Srivastava *et al.* proposed SPR gas sensor based on graphene in the THz band, this design can obtain maximum sensitivity (S) 52.7°/RIU [14]. Xiang *et al.* design a different structure for graphene-based terahertz gas sensor and get the highest sensitive 147°/RIU [15]. Comparing to noble metals, graphene has excellent optical performance and lower losses than metal in the THz band [16].

In this article, we propose the hybrid structure based on SPhP mode and SPP mode and realize the strong coupling between two different modes. The research about the coupling between different electromagnetic modes has learned more in the visible and THz band, such as Fano resonance based on graphene (SPP mode) and planar waveguide mode (PWG mode) [17], [18], strong coupling between PWG mode and long-range surface (LRSPP) [19] and so on. The two modes may couple together when the wave vector of SPhP mode (supported by the CsI) close to the SPP mode (supported by the graphene). We calculate the reflectance spectrum numerically and find that there is a narrow resonance and broad resonance on it at the same time. This phenomenon is called normal-mode splitting [20], which signifies the strong coupling SPhP mode and SPP mode.

2. Design Consideration and Theoretical Model

The proposed structure exhibits in the elementary diagram Fig. 1(c), we choose the Kretschmann configuration and the Germanium (the refractive index $n_p = 4$) as the coupling prism. The cesium iodide (CsI) layer is deposited onto the coupling prism, the coupling layer Air (the refractive index $n_{Air} = 1$) is between CsI layer and few-layer graphene (FLG), the yellow block represents the CsI layer. Fig. 1(a) is the traditional surface phonon resonance sensor based on CsI. Fig. 1(b) is the
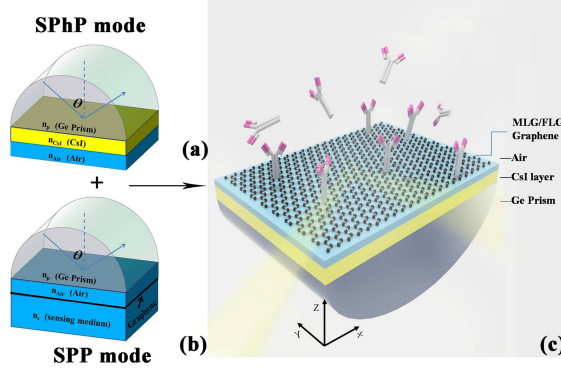
Fig. 1. (a) and (b) are the structure of SPhP mode based on CsI and SPP mode based on graphene. (c) The elementary diagram of the proposed terahertz sensor.

surface Plasmon resonance sensor based on graphene. As we think, it will be possible to realize the coupling of two modes of SPhP and SPP only if we choose the appropriate materials and the thickness of the coupling layer. Firstly, we need to verify that the two modes can be coupled by employing a monolayer graphene (MLG). In the theoretical simulation, we use the Fermi energy of graphene as $E_F = 0.85$ eV and the thickness of CsI as $d_{CsI} = 10$ μm.

We use the experimental date of cesium iodide as the calculation of the paper, the complex permittivity of CsI is given by [21]:

$$\varepsilon(\omega) = \varepsilon_\infty + (\varepsilon_{stat} - \varepsilon_\infty) \frac{\omega_{TO}^2}{(\omega_{TO}^2 - \omega^2 - i\omega\Gamma_{TO})}, \tag{1}$$

where $\varepsilon_\infty = 3.17$, $\varepsilon_{stat} = 6.03$, $\omega_{TO} = 2\pi \times 1.8 \times 10^{12}$ rad/s, and $\Gamma_{TO} = 0.3 \times 10^{12}$ rad/s, and the dispersion relation of SPhP mode can analogous to SPP mode, which can be defined as:

$$k_{spp}(\omega) = \frac{\omega}{c} \sqrt{\frac{\varepsilon_{CsI}(\omega)\varepsilon_{Air}(\omega)}{\varepsilon_{CsI}(\omega) + \varepsilon_{Air}(\omega)}}, \tag{2}$$

the angle frequency is ω, and light velocity is c in a vacuum.

We know the complicated surface conductivity $\sigma(\omega, \mu, \Gamma, T)$ of graphene is composed of two parts $\sigma = \sigma_{intra} + \sigma_{inter}$ (corresponding to intraband and interband), which can be deduced by Kubo formula [22]–[24].

$$\sigma_{intra} = i\frac{e^2 K_B T}{\pi\hbar^2(\omega + i\tau)} \left[\frac{E_F}{K_B T} + 2\ln(e^{-\frac{E_F}{K_B T}} + 1) \right], \tag{3}$$

$$\sigma_{inter} = i\frac{e^2}{4\pi\hbar} \ln \left| \frac{2E_F - (\omega + i\tau)\hbar}{2E_F + (\omega + i\tau)\hbar} \right|, \tag{4}$$

In this article, we set the phenomenological relaxation time as $\tau = 0.1$ ps, other parameters can be derived from references. For all we know that graphene can support TM SPPs and behave metal properties only the imaginary component of conductivity is positive. The SP dispersion of air-MLG-sensing medium system can be deduced as [25], [26]:

$$\frac{n_1^2}{k_{z1}} + \frac{n_2^2}{k_{z2}} + \frac{i\sigma}{\omega\varepsilon_0} = 0, \tag{5}$$

where $k_{zi} = \sqrt{k_{sp}^2 - n_i^2 k_0^2}$ and $i = \{1.2\}$ is the transverse wave number of SPPs.

For calculating the variation of reflectivity of the designed multilayer configuration, we can obtain the angular spectrum after calculation and theoretic modeling from Fresnel equations and the transfer matrix method (TMM) [9], [27], 28], which is a function of the angle of incidence θ_{in}. We
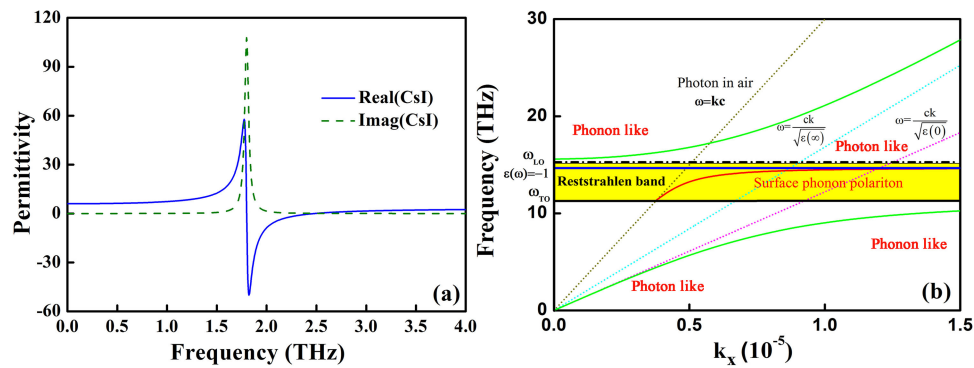
Fig. 2. (a) The real and imaginary parts of the permittivity of CsI. (b) The dispersion relationship of Phonon polariton for CsI for bulk and surface phonon polaritons (corresponding to the green and red line). The black lines correspond to the frequency locations of the LO and TO phonon frequencies. The yellow areas denote the reststrahlen band and the orange dashed line corresponds to the dispersion of photons in the air, the blue and pink line (the high and low-frequency limit of CsI) are provided for comparison.

can see from the proposed configuration, all layers are stacked along the direction perpendicular to the prism, and each layer is defined by the thickness, refractive index, and dielectric constant, respectively. Therefore, we employ the TMM to analyze the reflectance of the incident TM-polarized light. We employ a sensitivity by the intensity in this article, which is defined as $S = dR_p/dn_s$ [29], For the fixed change of the refractive-index $\triangle n_s$, the larger $\triangle R_p$ is, the larger the sensitivity S is. In the final, we also discuss the full width at half maximum (FWHM), detection accuracy ($DA = 1/FWHM$) and the figure of merit (FOM = S·DA) to define the performance of the proposed structure [30].

3. Numerical Results and Discussions

The real and imaginary parts of the dielectric functions curves of CsI, following the mode of [21]. The existing condition of the surface polaritons is that the real part of the dielectric function supporting the materials on both sides of the surface polariton is opposite sign, and the real part of the negative dielectric function is usually accompanied by the dielectric anomaly [31]. We could find the surface phonon polariton can be generated when the real part of CsI dielectric function from Fig. 2(a). Fig. 2(b) is the schematic diagram of the dispersion of phonon-polariton, we can see the picture is divided into phonon like area and photon area firstly, the most notable feature is the electromagnetic waves cannot propagate in crystals within the limit of frequency band ω_{TO} and ω_{LO}, ω_{TO} and ω_{LO} are the longitudinal and transverse optical phonon frequencies, respectively, the relationship between them can be defined as the function of high-(ε_∞) and low-frequency (ε_0), which is $(\omega_{LO}/\omega_{TO})^2 = \varepsilon_0/\varepsilon_\infty$, dielectric function is negative and the wave vector is imaginary number in the wave or frequency band, external radiation incident on the crystal is completely reflected in this frequency range If we neglect damping effect, this frequency range is known as reststrahlen band. We can take advantage of this feature to get quasi-monochromatic light and attribute this effect to enter the artificial band gap ranks with photonic crystal and photonic crystal.

Before starting work, it is necessary for us to prove whether the two modes can be coupled and plot the effective refractive index varying with E_F in Fig. 3(a). We could see the orange straight line corresponds to the configuration of Ge prism-CsI-air because the effective refractive index of CsI doesn't change with E_F. The black dashed line corresponds to the structure of Prism-Air-MLG-sensing medium and demonstrates graphene with excellent tunability in the THz band. We can see from the diagram that two lines intersect at a point when E_F is 0.85 eV (he source excitation frequency is 2.3 THz), which means the two modes can be coupled. Then we plot the angular spectrum of reflectance solely graphene SPP and CsI SPhP mode (the inside figure is corresponding to the excitation structure) in Fig. 3(b) and 3(c), we're moving two resonant angles into the adjacent area (shown as point B and A). When these two modes are coupled, it is found
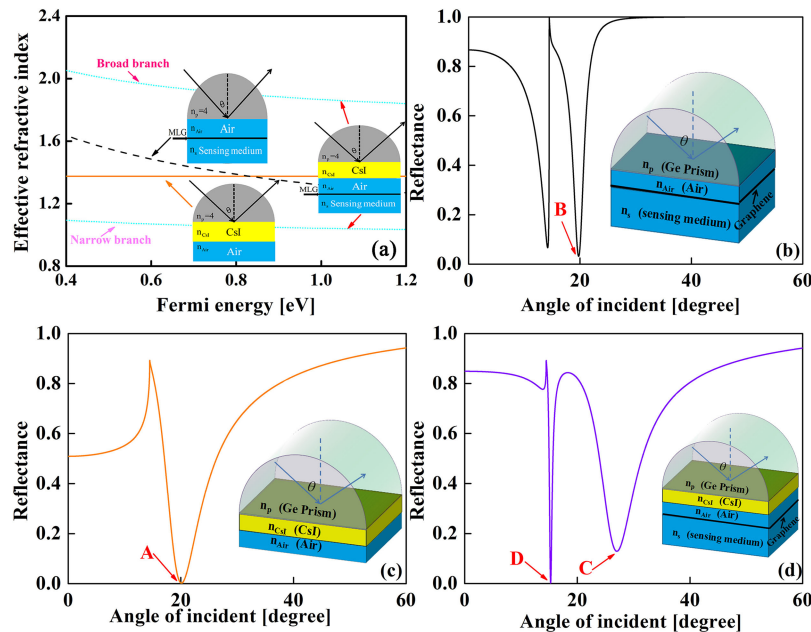
Fig. 3. (a) Effective refractive indices of sole SPhP for CsI mode (orange line) and graphene mode (black dashed line), and the coupling of CsI with graphene mode resulting two branches (blue dotted line). Adjust the resonant angles of the two modes of MLG and CsI separately and make them at the near position, when $E_F = 0.85$ eV, $f = 2.3$ THz, $d_{Air} = 20$ μm, and $d_{CsI} = 10$ μm, the inside figure corresponds to the structure respectively, (b), (c) and (d) is the angular spectrum of sole graphene SPP and sole CsI SPhP and the coupling of two modes.

that there are two resonances (15.2° and 28.9°) on the reflectance spectrum, one resonance angle is narrow and the other is broader as Fig. 3(d) shown, and both of them deviate from the original resonance position (correspond the point A and B). This phenomenon is known as normal-mode coupling or splitting. In Fig. 3(a), the anti-crossing curve (blue dotted lines) is calculated by measuring the resonant angles, which is the corresponding to the narrow and broad resonance in Fig. 3(d). It is obvious that the narrow resonance is highly sensitive in the variation of substrate-specific refractive power.

After realizing the excitation of sole SPhP mode and SPP mode by theoretical simulation, we find out the two modes can be coupled together resulting in a narrow and a broad branch, then should further illustrate the origin of the four dips denoted as "A", "B", "C" and "D" in Fig. 3 and plot the distribution of the electric field. It is distinctly different from the distribution profile that the distribution electric field concentrates within a certain region. The Fig. 4(a) and 4(b) corresponds to the dip "A" and "B", figure exhibits that large electric field enhancement firstly appears around the CsI-Air layer surface and Air-graphene-air surface then decreases exponentially far from the interface respectively, which has shown the excitation of SPP and SPhP modes. The Fig. 4(c) and 4(d) corresponds to the dip "C" (narrow branch) and "D" (broad branch), the field intensity has significant enhancement in the surface of CsI-Air and Air-graphene-air from the picture (c), which results in the narrow branch after the two modes couple together. We can clearly see that the field strength of CsI is much larger than graphene, we know the reason for the enhancement of SPP due to the enhancement of the electric field, the sensor will be sensitive in the variation index of refraction of the substrate, on account of the small change of the refractive index of sensing medium near the interface may result a larger change in the characteristics of surface wave, then the strength of the electric field will be changed [32], [33]. The broad branch originates large loss of CsI.

After figuring out the two modes (SPhPs mode and SPPs mode) can be coupled together and the origin of narrow and broad resonance, we should optimize the parameters of a proposed
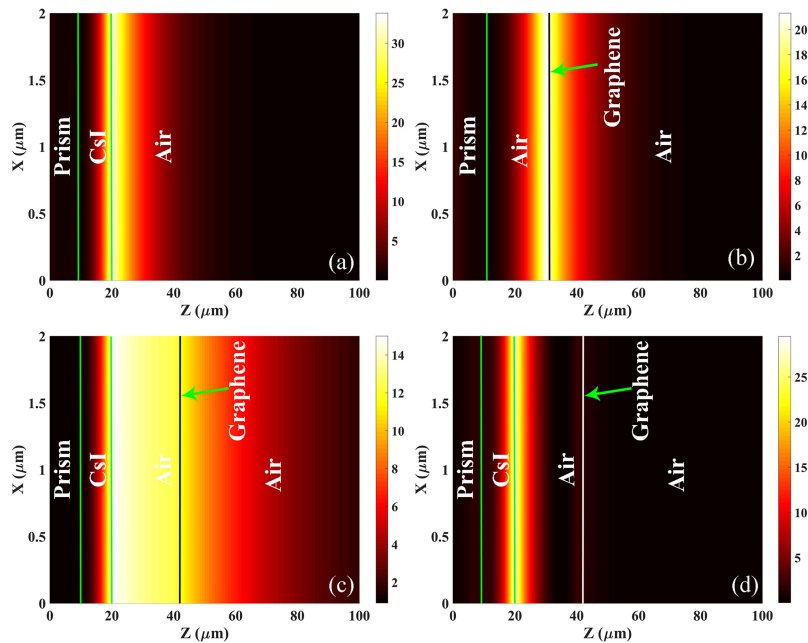
Fig. 4. The electric field distributions along the direction perpendicular to the prism for SPhP mode of (a) CsI and SPP mode of (b) graphene; electric field distributions at (c) $\theta = 15.2°$ and (d) $\theta = 28.9°$ when CsI is coupled with grapheme.

multilayer structure in order to gain the best performance. It is known to all that the dielectric layer thickness is also an important factor to affect the performance of the proposed configuration, therefore discuss the influence to constantly change the thickness of d_{Air}. We could suppose that the coupling between two modes was impossible to happen when the coupling layer with huge thickness, if we bring the two modes closer together we could discover a narrow resonance and a broad resonance, and continuing to decrease the coupling layer, we can find the narrow resonance become narrower, meanwhile, the broad resonance disappears (means becoming much broader) in the angular spectrum from the Fig. 5(a). The enlarge figure with the incident angle changing 14.7° from 15.8° in Fig. 5(b). Fig. 5(c) and 5(d) shows the variation of the FWHM, DA, sensitivity, and FOM with the decreasing of the thickness of the coupling layer for the proposed configuration. It illustrates that FWHM (Fig. 5(c)) is narrower and narrower with the decreasing coupling layer thickness, thence a larger DA (Fig. 5(b)) can be obtained. Although Fig. 5(d) has shown the decrease of sensitivity with the increase of dielectric thickness, while FOM for the proposed SPR sensor is enhanced due to the large DA.

Moreover, the layer of graphene is also an important factor to affect the performance of the proposed structure. Here, we regard individual graphene sheet as a non-interacting monolayer and the optical conductive of the few-layer graphene (FLG) is $N\sigma$, where N is the number of layers (N < 6) and then we plot the variation of FWHM, DA, sensitive and FOM with the changing thickness of coupling layer and different graphene layer [24]. It illustrates that FWHM (Fig. 6(a)) is narrower and narrower with the increasing graphene layer and decreasing dielectric thickness, thence a larger DA (Fig. 6(b)) can be obtained. The sensitive (Fig. 6(c)) get maximum value When graphene layer N = 5 and the thickness of coupling layer is $d_{Air} = 0$ μm, which suggests that the coupling layer (Air layer) is an assumption and inexistent, and the FLG can be directly coated on the surface of CsI layer. In the finally, a large FOM as high as 74740 RIU^{-1} can be received.

It is all known that refractive index of sensing medium may have a slight change when there are chemical reaction and biological action in sensing medium. Fig. 7(a) and 7(b) show the variation of FWHM, DA, sensitivity, and FOM with the refractive index of sensing medium change from 1.00 to 1.08 for $d_{Air} = 0$ and graphene layer N = 5. It clear illustrates that FWHM is becoming broader
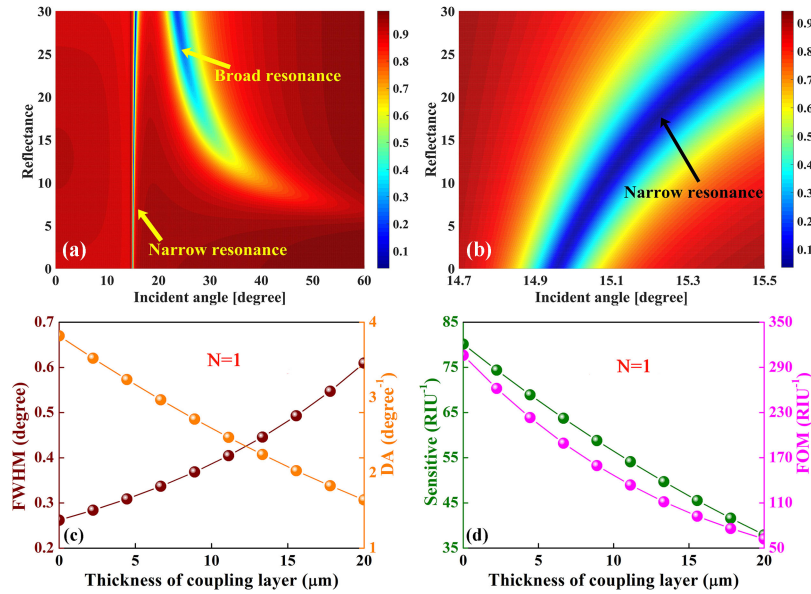
Fig. 5. (a) Variation of reflectance with the thickness of the coupling layer for the proposed structure, (b) the enlarged view with the angle varying 14.7° from 15.5°. Variation of the FWHM, DA (c), sensitivity and FOM (d) with the changing of the thickness of coupling layer when graphene layer is N = 1.
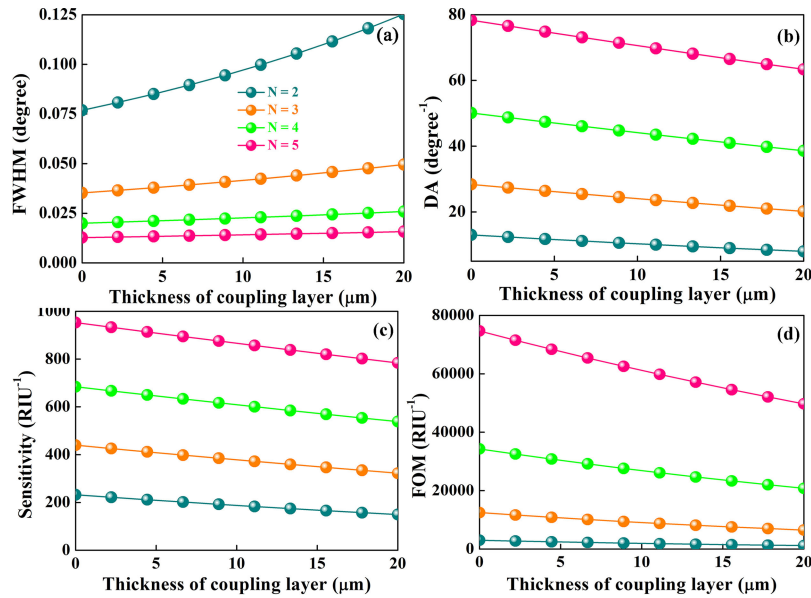

Fig. 6. (a) Variation of the (a) FWHM, (b) DA, (c) sensitivity and (d) FOM with the increase of dielectric thickness for the proposed structure for different graphene layer N = 2,3,4,5.

with the refractive index of sensing medium change from 1.00 to 1.08, while DA, sensitivity, and FOM can be decreased with the increasing RI of sensing medium. And we believe that this novel structure based on strong coupling between different modes can play an important role in THz optical sensing technology.

In the final section, it is listed some of the recent work about related materials and coupling between two different modes in the Table 1. A high figure of merit (FOM) 74740 can be obtained for the proposed structure. With such excellent performance, we believe that this scheme could be
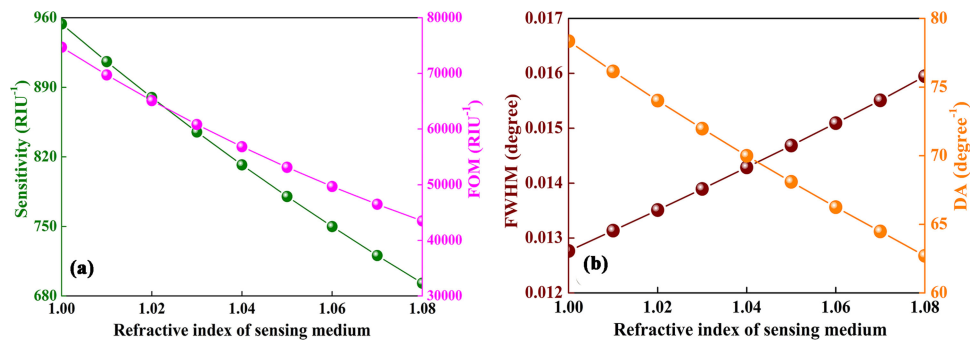
Fig. 7. (a) and (b) Variation of the sensitivity, FOM, FWHM and DA with the refractive index of sensing medium change from 1.00 to 1.08 for $d_{Air} = 0$ and graphene layer N $=$ 5.

TABLE 1

Sensitivity Comprise With Recent Work

Ref	Frequence (THz)	Maximum FOM (RIU⁻¹)
Wang et al. [18]	28.3	140
Srivastava et al. [14]	5.0	741
Zheng et al. [34]	27.8	72160
Proposed scheme	2.3	74740

found potential applications in the chemical examination, medical diagnosis, and biological detection *etc*.

4. Conclusion

In conclusion, we proposed a well-designed intensity-interrogated terahertz sensor based on the Kretschmann configuration consisting of a germanium prism and multilayer thin film, to realize the strong coupling between two different modes. Based on the numerical analysis, the highest imaging sensitivity of 954 RIU^{-1} is realized for our design structure. We firstly employ the method of the effective refractive index to verify the coupling between different modes and then research the origin of the resonance dip by plotting the electric field distributions. In the final section, we optimize the structure to get satisfying performance parameters of the proposed structure. We hope that our novel designs could play a significant role in optical sensing technology in terahertz band.

References

[1] R. Bogue, "Sensing with terahertz radiation: A review of recent progress," *Sensor Rev.*, vol. 38, no. 6, pp. 216–222, 2018.
[2] S. Dhillon *et al.*, "The 2017 terahertz science and technology roadmap," *J. Phys. D: Appl. Phys.*, vol. 50, no. 4, Jan. 2017, Art. no. 043001.
[3] P. Logofatu and V. Damian, "Super-resolution terahertz imaging by subpixel estimation: Application to hyperspectral beam profiling," *J. Opt.*, vol. 20, no. 5, Apr. 2018, Art. no. 055701.
[4] X. Dai, L. Jiang, and Y. Xiang, "Tunable optical bistability of dielectric/nonlinear graphene/dielectric heterostructure," *Opt. Express*, vol. 23, no. 5, pp. 6497–6508, Mar. 2015.
[5] D. Ha, D. Thuy, V. Hoa, T. Van, and N. Viet, "On the theory of three types of polaritons (phonon, exciton, and plasmon polaritons)," *J. Phys.: Conf. Ser.*, vol. 865, 2017, Art. no. 012007.
[6] M. Haraguchi, M. Fukui, and S. Muto, "Experimental observation of attenuated-total-reflection spectra of GaAs/AlAs superlattice," *Phys. Rev. B Condens. Matter*, vol. 41, no. 2, pp. 1254–1257, Jan. 1990.

[7] G. Dayal, X. Y. Chin, C. Soci, and R. Singh, "High-Q plasmonic Fano resonance for multiband surface-enhanced infrared absorption of molecular vibrational sensing," *Adv. Opt. Mater.*, vol. 5, no. 2, Jan. 2017, Art. no. 1600559.

[8] T. Silans *et al.*, "Temperature dependence of the dielectric permittivity of CaF_2, BaF_2, and Al_2O_3: Application to the prediction of a temperature-dependent van der Waals surface interaction exerted onto a neighboring $Cs(8P_{3/2})$ atom," *J. Phys. Condens. Matter*, vol. 21, no. 25, May 2009, Art. no. 255902.

[9] J. Homola, S. Yee, and G. Gauglitz, "Surface plasmon resonance sensors: Review," *Sensors Actuators B: Chem.*, vol. 54, pp. 3–15, Jan. 1999.

[10] A. Otto, "Excitation of nonradiative surface plasma waves in silver by the method of frustrated total reflection," *Zeitschrift für Physik*, vol. 216, no. 4, pp. 398–410, 1968.

[11] A. K. Sharma, R. Jha, and B. D. Gupta, "Fiber-optic sensors based on surface plasmon resonance: A comprehensive review," *IEEE Sensors J.*, vol. 7, no. 7–8, pp. 1118–1129, Aug. 2007.

[12] A. Vakil and N. Engheta, "Transformation optics using graphene," *Science*, vol. 332, no. 6035, pp. 1291–1294, Jun. 2011.

[13] F. Bonaccorso, Z. Sun, T. Hasan, and A. C. Ferrari, "Graphene photonics and optoelectronics," *Nature Photon.*, vol. 4, no. 9, pp. 611–622, Aug. 2010.

[14] T. Srivastava, A. Purkayastha, and R. Jha, "Graphene-based surface plasmon resonance gas sensor for terahertz," *Opt. Quantum Electron.*, vol. 48, no. 6, p. 334, Jun. 2016.

[15] Y. Xiang, J. Zhu, L. Wu, Q. You, B. Ruan, and X. Dai, "Highly sensitive terahertz gas sensor based on surface plasmon resonance with graphene," *IEEE Photon. J.*, vol. 10, no. 1, Feb. 2018, Art. no. 6800507.

[16] A. K. Geim and K. S. Novoselov, "The rise of graphene," *Nature Mater.*, vol. 6, no. 3, pp. 183–191, Mar. 2007.

[17] B. Ruan *et al.*, "Ultrasensitive terahertz biosensors based on Fano resonance of a graphene/waveguide hybrid structure," *Sensors*, vol. 17, no. 8, p. 1924, Aug. 2017.

[18] J. Wang, C. Song, J. Hang, Z. Hu, and F. Zhang, "Tunable Fano resonance based on grating-coupled and graphene-based Otto configuration," *Opt. Express*, vol. 25, no. 20, pp. 23880–23892, Sep. 2017.

[19] L. Wu, J. Guo, H. Xu, X. Dai, and Y. Xiang, "Ultrasensitive biosensors based on long-range surface plasmon polariton and dielectric waveguide modes," *Photon. Res.*, vol. 4, no. 6, pp. 262–266, Oct. 2016.

[20] G. Khitrova, H. M. Gibbs, F. Jahnke, M. Kira, and S. W. Koch, "Nonlinear optics of normal-mode-coupling semiconductor microcavities," *Rev. Modern Phys.*, vol. 71, no. 5, pp. 1591–1639, Oct. 1999.

[21] J. Knab, A. Adam, E. Shaner, H. Starman, and P. Planken, "Terahertz near-field spectroscopy of filled subwavelength sized apertures in thin metal films," *Opt. Express*, vol. 21, no. 1, pp. 1101–1112, Jan. 2013.

[22] P. Chen and A. Alu, "Atomically thin surface cloak using graphene monolayers," *ACS Nano*, vol. 5, no. 7, pp. 5855–5863, Jul. 2011.

[23] G. W. Hanson, "Dyadic Green's functions and guided surface waves for a surface conductivity model of graphene," *J. Appl. Phys.*, vol. 103, no. 6, Mar. 2008, Art. no. 064302.

[24] J. Guo, L. Jiang, X. Dai, and Y. Xiang, "Tunable Fano resonances of a graphene/waveguide hybrid structure at a mid-infrared wavelength," *Opt. Express*, vol. 24, no. 5, pp. 4740–4748, Feb. 2016.

[25] C. H. Gan, "Analysis of surface plasmon excitation at terahertz frequencies with highly doped graphene sheets via attenuated total reflection," *Appl. Phys. Lett.*, vol. 101, no. 11, Sep. 2012, Art. no. 11609.

[26] H. Xu, L. Wu, X. Dai, Y. Gao, and Y. Xiang, "An ultra-high sensitivity surface plasmon resonance sensor based on graphene-aluminum-graphene sandwich-like structure," *J. Appl. Phys.*, vol. 120, no. 5, Aug. 2016, Art. no. 053101.

[27] B. D. Gupta and A. K. Sharma, "Sensitivity evaluation of a multi-layered surface plasmon resonance-based fiber optic sensor: A theoretical study," *Sensors Actuators B: Chem.*, vol. 107, no. 1, pp. 40–46, May 2005.

[28] L. Wu, H. S. Chu, W. S. Koh, and E. P. Li, "Highly sensitive graphene biosensors based on surface plasmon resonance," *Opt. Express*, vol. 18, no. 4, pp. 14395–14400, Jun. 2010.

[29] R. Verma, B. D. Gupta, and R. Jha, "Sensitivity enhancement of a surface plasmon resonance based biomolecules sensor using graphene and silicon layers," *Sensors Actuators B: Chem.*, vol. 160, no. 1, pp. 623–631, Dec. 2011.

[30] D. Kaur, V. K. Sharma, and A. Kapoor, "High sensitivity lossy mode resonance sensors," *Sensors Actuators B: Chem.*, vol. 198, pp. 366–376, Jul. 2014.

[31] T. Low *et al.*, "Polaritons in layered two-dimensional materials," *Nature Mater.*, vol. 16, no. 2, pp. 182–194, Nov. 2017.

[32] P. K. Maharana, R. Jha, and S. Palei, "Sensitivity enhancement by air mediated graphene multilayer based surface plasmon resonance biosensor for near infrared," *Sensors Actuators B: Chem.*, vol. 190, no. 1, pp. 494–501, Jan. 2014.

[33] L. Wu *et al.*, "Sensitivity enhancement by using few-layer black phosphorus-graphene/TMDCs heterostructure in surface plasmon resonance biochemical sensor," *Sensors Actuators B: Chem.*, vol. 249, pp. 542–548, Oct. 2017.

[34] G. Zheng, Y. Chen, L. Bu, L. Xu, and W. Su, "Waveguide-coupled surface phonon resonance sensors with super-resolution in the mid-infrared region," *Opt. Lett.*, vol. 41, no. 7, pp. 1582–1585, Apr. 2016.